

---

# EXPLOITING FULL RESOLUTION FEATURE CONTEXT FOR LIVER TUMOR AND VESSEL SEGMENTATION VIA FUSION ENCODER: APPLICATION TO LIVER TUMOR AND VESSEL 3D RECONSTRUCTION

---

A PREPRINT

**Xiangyu Meng**<sup>\*</sup>

Department of Computer Science and technology  
China University of Petroleum  
Qingdao 266580, Shandong, China  
xiangyumeng@s.upc.edu.cn

**Xudong Zhang**<sup>\*</sup>

Department of Computer Science and technology  
China University of Petroleum  
Qingdao 266580, Shandong, China  
bigdongsir@163.com

**Gan Wang**

Department of Computer Science and technology  
China University of Petroleum  
Qingdao 266580, Shandong, China  
s20070048@s.upc.edu.cn

**Ying Zhang**

Department of Computer Science and technology  
China University of Petroleum  
Qingdao 266580, Shandong, China  
zhangy9808@163.com

**Xin Shi**

Department of Computer Science and technology  
China University of Petroleum  
Qingdao 266580, Shandong, China  
shix1104@163.com

**Huanhuan Dai**

Department of Computer Science and technology  
China University of Petroleum  
Qingdao 266580, Shandong, China  
daihuanhuan0901@163.com

**Zixuan Wang**<sup>†</sup>

Minimally Invasive Interventional Therapy Center  
Qingdao Municipal Hospital  
Qingdao 266011, Shandong, China  
prince\_room@sina.com

**Xun Wang**<sup>†</sup>

Department of Computer Science and technology  
China University of Petroleum  
Qingdao 266580, Shandong, China  
wangsyun@upc.edu.cn

November 29, 2021

## ABSTRACT

Liver cancer is one of the most common malignant diseases in the world. Segmentation and labeling of liver tumors and blood vessels in CT images can provide convenience for doctors in liver tumor diagnosis and surgical intervention. In the past decades, automatic CT segmentation methods based on deep learning have received widespread attention in the medical field. Many state-of-the-art segmentation algorithms appeared during this period. Yet, most of the existing segmentation methods only care about the local feature context and have a perception defect in the global relevance of medical images, which significantly affects the segmentation effect of liver tumors and blood vessels. We introduce a multi-scale feature context fusion network called TransFusionNet based on Transformer and SEBottleNet. This network can accurately detect and identify the details of the region of interest of the liver vessel, meanwhile it can improve the recognition of morphologic margins of liver tumors

---

<sup>\*</sup>These authors contributed equally

<sup>†</sup>Corresponding author

by exploiting the global information of CT images. Experiments show that TransFusionNet is better than the state-of-the-art method on both the public dataset LITS and 3Dircadb and our clinical dataset. Finally, we propose an automatic 3D reconstruction algorithm based on the trained model. The algorithm can complete the reconstruction quickly and accurately in 1 second.

**Keywords** Liver tumor and vessel · CT segmentation · Fusion encoder · 3D reconstruction

## 1 Introduction

Liver cancer is the sixth most common primary cancer worldwide and the fourth leading cause of cancer death[1]. Therefore, there is an urgent need for effective prevention programs and treatments to reduce the harm caused by liver cancer. In the early stage of liver cancer, potential risks of coming serious liver cancer can be eliminated by surgical removal of the tumor or local treatment. In recent years, computer-assisted liver surgery (e.g., ablation and embolization) has been increasingly used for the treatment of primary and secondary liver tumor patients who are not eligible for common surgeries[2]. Computed Tomography(CT), as part of computer-assisted liver surgery, is a commonly implemented for clinical diagnostic approach to improve the visualization on liver, vessels and tumors[3]. Because CT is capable of clearly showing the number, boundary, density and other patterns of the disease focus. Experts will segment liver vessels and tumors from CT images before surgery in helping 3D visualization, path planning, and guidance for interventional surgery of liver[4]. However, there are some challenging obstacles in computer-assisted liver interventions. The most critical one of all is that segmentation of liver vessels and tumors from CT images is manually completed by specialists, which is rather time-consuming, labor-intensive and no quality guaranteed. This can lead to the inability to precisely pinpoint the vessels that supplies nutrition for the hepatic tumor, thus affecting hepatic embolization procedure, ablation and so on. Eventually local tumors will relapse[5] . As a result, there is an urgent clinical need for techniques that can automatically, accurately and rapidly segment liver tumors and their supplying vessels.

In previous studies, many methods have emerged for segmenting liver vessels separately or tumors as well, but none of which considers segmenting vessels and tumors at the same time. This is due to the complicated background, heterogeneous shape and surrounding vessels irregularity of the tumor making it difficult to segment the hepatic vessels that supply nutrition for the tumor[6]. Traditional methods try to segment livers or tumors by active contour methods, tracking methods, and feature learning methods. Active Contour Model (ACM) is a method to detect object boundaries based on curve evolution theory and level set approach. Cheng et al. [7] implemented ACM with precise shape dimension constraints based on CT scan models for contour point detection of vessel cross-sections to plot vessel boundaries. Chung et al. [8] proposed an active contour method to segment portal vein and hepatic vein based on the regional intensity distribution of the image and the probability map of vessel occurrence. However, the active contour model tends to fall into the local optimum problem when extracting complex regions in the vector field, and cannot handle gray scale inhomogeneous images well. The tracing method starts by manual initialization or image preprocessing to initiate a single or specified number of seed points in the vessel, and then finds subsequent points based on the image derived data as a way to trace the vessel[3]. Tracking methods mainly include model-based algorithms [9, 10, 11],least cost path-based algorithms [12, 13]. However, if the initial seed points of these methods are not correctly positioned, the final segmentation results can be seriously affected.

In order to segment vessels or tumors from CT images, feature learning methods need to perform feature extraction from images and labels based on real segmentation to train machine learning models such as random forest (RF) [14, 15] and support vector machine (SVM) [16, 17] for automatically segmenting vessels or tumors from CT images. However, the robustness and generalization ability of machine learning models are limited. In recent years, many deep learning models ,like convolutional neural networks [18, 19, 20],have gradually shown promosing performances in the field of medical image segmentation. Currently, segmentation models based on fully convolutional networks [21] and UNet [22] architectures are the most effective ones. Huang et al. [23] combined 3D-UNet with data enhancement techniques, a variant of dice coefficient, to reduce the effect of high imbalance in some extent between hepatic vessels and background classes. Zhou et al. [24] proposed UNet++, a model that combines a deeply supervised encoder and decoder and links the sub-networks of both through a series of hops as a way to reduce the semantic gap between the encoder and decoder feature mappings. Recently, Transformer [25] has made great achievements in the field of deep learning, and TransUNet proposed by Chen et al. applies transformer as an encoder to extract global contextual features and combines it with convolutional neural network for decoding. For segmentation of liver vessels and tumors, a high degree of accuracy must be achieved to enable clinical applications. In view of above mentioned methods including other UNet-based [26, 27, 28] methods , performances still can be improved in terms of accuracy and efficiency despite of some attempts in architecture.

In our work, we construct a general semantic segmentation model TransFusionNet according to the different semantic features of liver tumors and vessels in CT images. It is a multiscale information fusion network capable of learning global and local information features, including a Transformer-based global feature encoder, a multilayer SEBottleNet residual stacking-based local feature encoder, and a multiscale fusion decoder. The model can accurately detect and segment fine-scale arterial vasculature, while effectively identifying and segmenting liver tumors and vascular features by fusing the global context of CT images. In addition, since images obtained from different scanners or different imaging protocols during clinical diagnosis. Instead, training of deep learning models often requires a large amount of labeled data that is supposed to accurately represent the original data[29]. To tackle this problem, we propose transfer learning for image segmentation by pre-training TransFusionNet through two publicly available datasets with a large sample size, and then fine-tuning the training on an actual clinical dataset with a smaller sample size. In this way, we resolve the differences between the previous distribution of training and original data which reduce the difficulties arising from cross scanner and protocols and alleviate the influence of small clinical data samples.

## 2 Methods

Given a CT image  $x \in \mathbb{R}^{H \times W \times C}$  with spatial resolution of  $H \times W$  which consists of  $C$  channels, the goal is to feed it into the TransFusionNet model for label map prediction. TransFusionNet is a segmentation model that can learn global and local information features in multi-dimensions, which can accurately detect and segment tiny arterial vessel and liver tumor. The framework of our model is shown in Figure 1.

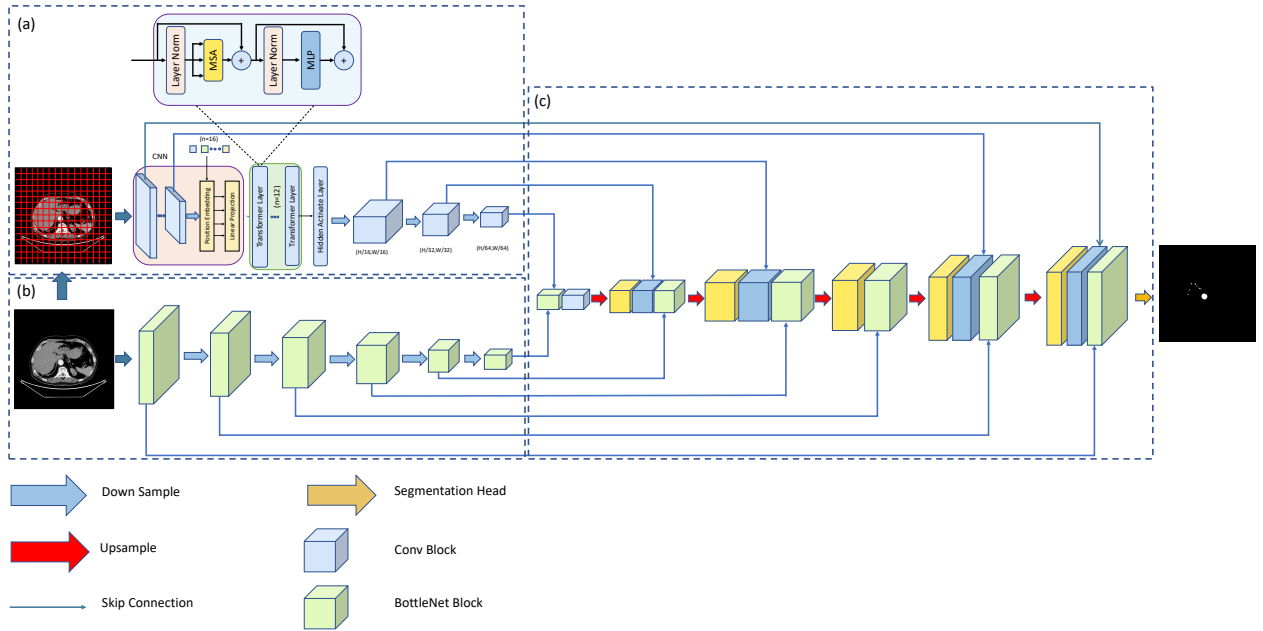


Figure 1: Overview of the TransFusionNet model. (a) Transformer-based encoder for global feature (b) SEBottleNet-based encoder for local feature (c) Fusion decoder for multiscale feature.

### 2.1 Transformer-based global feature encoder

We introduce an encoder that can learn the global feature representation, which consists of a backbone feature embedding module based on deep convolutional network ResNet50 [28] and a feature extraction module that senses the global information representation of the image based on the transformer [25]. This module adopts a brand-new feature extraction idea, by semantically representing the features of the picture and learning the global representation of semantic features. A multi-layer residual networks stacked together in ResNet50 backbone feature embedding module, which continuously fuses feature information from local receptive fields and learns more diverse feature representations. We divide the feature map  $x \in \mathbb{R}^{H' \times W' \times C'}$  learned by ResNet50 into a series of patches  $x_p^i \in \mathbb{R}^{P^2 \times C}$ ,  $i = 1, \dots, N$ , where the size of each patch is  $P \times P$ , and the number of patches denote by  $N = \frac{H' \times W'}{P^2}$ . For each patch, we use a convolution operation with a kernel size of  $P \times P$  to obtain the information  $E_{info}^i$  of  $i$ -th patch to form an

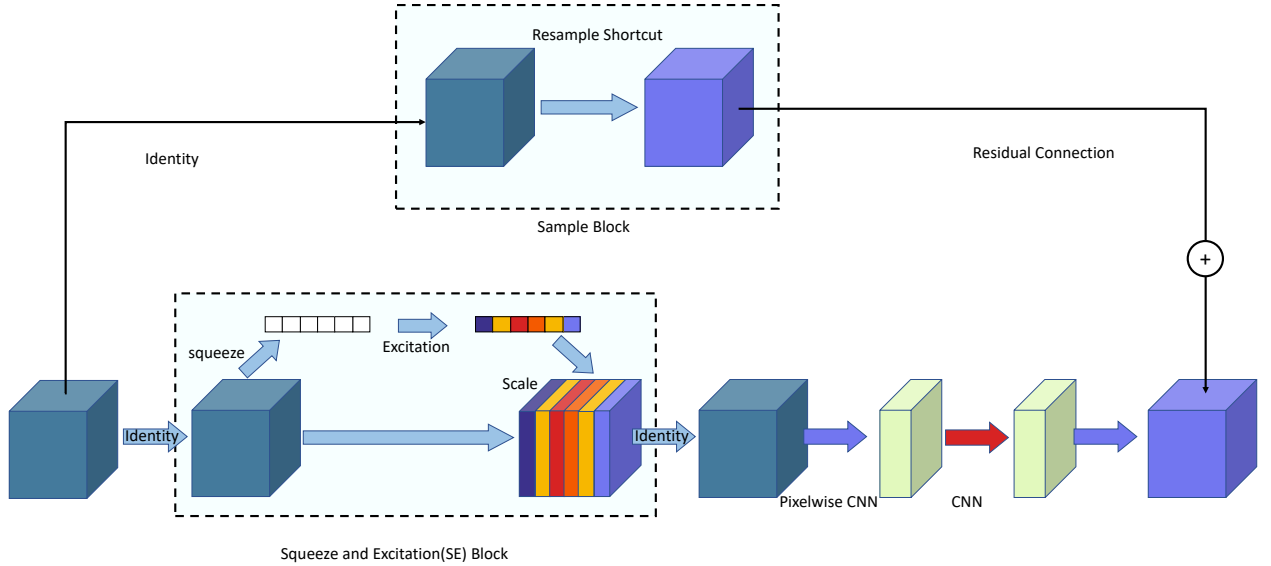


Figure 2: Bottleneck network structure with SE block

information matrix  $\{E_{info}^1, E_{info}^2, \dots, E_{info}^N\}$ . In order to better learn location information using Transformer, we perform a learnable location embedding for each patch to obtain the location matrix  $\{E_{pos}^1, E_{pos}^2, \dots, E_{pos}^N\}$  of the  $N$  patches. The feature of the  $i$ -th patch can be formulated by the following equation:

$$E^i = E_{info}^i + E_{pos}^i. \quad (1)$$

We next input the above obtained feature matrix  $E = \{E^1, E^2, \dots, E^N\}$  of  $x$  into multi Transformer layers to learn global feature information. In comparison to traditional convolution operation, transformer adopts a multi-head self-attention mechanism, and its core formulation is shown in equation 2:

$$y = \sum_{i=1}^h \sum_{j=1}^w \sum_{k=1}^n (\text{softmax}(Q_{ijk}^T \times K_{ijk}) \times V_{ijk}), \quad (2)$$

where  $h$  and  $w$  denote by width and height of the feature matrix  $E$  after feature extraction and location embedding. And  $n$  is the number of self-attention mechanism heads.  $Q_{ijk}, K_{ijk}, V_{ijk}$  denote the query, key and value obtained by three linear transformations of the input  $E_{ij}$  in each self-attended head, respectively.  $y \in \mathbb{R}^{hwC}$  denotes the output after one multi-headed self-attention. We stacked 12 transformer layers, and the output of the last layer can theoretically learn to incorporate a rich global context feature representation of the CT image under a wider range of perceptual fields. We then feed the output of the Transformer layers into a three-layer convolution operation. The final encoded feature map consist global high-level abstract information, effectively solving the problem of missing information caused by perceptual field defects in traditional deep CNN networks.

## 2.2 Multi-layer SEBottleNet residual stacking for local feature information encoding network

Transformer-based encoder is a very powerful global information feature extractor, because transformer can better extract feature association information. In many ways, however, Transformer is not an effective replacement for traditional convolutional operations. For extraction of more subtle feature in some images such as edge feature of interest regions and tiny vessel feature, CNN is nothing but the perfect solution. We designed a local residual network encoder based on multi-layer SEBottleNet stacking, as shown in Figure 2. The encoder consists of a six feature extraction module. A max pooling operation is performed to extract the high-level feature representation after feed feature map to each feature extraction block. The input CT image  $x \in \mathbb{R}^{H \times W \times C}$  is first feed forward to a CNN module for high-level feature extraction, and the feature map  $u \in \mathbb{R}^{H \times W \times C_{>3}}$  is obtained, Where  $C_{>3}$  represents the channel of the feature map, and its number is greater than 3. Then, the feature map  $u$  is feed into a deep residual feature extractor stacked by five layers of SEBottleNet, each of which is used for learning the context features under the local perception field. Bottleneck residual network[30] retains all the advantages of residual network and significantly reduces

computation interval and computational burden. We introduced the Squeeze and Excitation(SE)[31] in the BottleNet to enhance the interdependence between feature map channels. The structure of the SEBottleNet is shown as in Fig. 2. The mean value  $e_c \in \mathbb{R}^{1 \times 1 \times C}$  of the feature embedding for each channel in the feature map  $U \in \mathbb{R}^{H \times W \times C}$  can be obtained from the Squeeze section, as shown in the following equation:

$$e_c = F_{sq}(u_c) = \frac{1}{w \times h} \sum_{i=1}^w \sum_{j=1}^h u_c(i, j). \quad (3)$$

Where the  $u_c(i, j) \in \mathbb{R}^{1 \times 1 \times C}$  is the pixel in feature map  $U$ . The Excitation section can learn the feature weights  $e_c$  for each channel by  $s_c$ :

$$s_c = F_{ex}(e_c, W) = \delta(\mathcal{G}(e_c, \mathcal{W})) \quad (4)$$

Finally, the vector product  $\tilde{O}$  of  $s$  and  $u$  is obtained by the Scale operation, and this is the final output of the SE module:

$$\tilde{O}_c = F_{scale}(e_c, s_c) = s_c \times u_c \quad (5)$$

where  $\tilde{O}_c$  is the feature map of a feature channel.

The SEBottleNet residual network splits the traditional convolutional operation into multiple modules to ensure that each module has a different feature extraction task. We introduced the Squeeze and Excitation module in the middle of the module to better learn the importance of the feature map channel dimensions, so that SEBottleNet has a stronger learning focus in the feature extraction process. Through the continuous stacking of SEBottleNet and maxpool, the encoder can continuously extract the local feature representation of the input CT image HIGH-level. Meanwhile, since each SEBottleNet is set with residual connections, it enables the encoder to effectively mitigate the degradation problem caused by network deepening.

### 2.3 Multi-scale feature fusion decoder network

In the previous two sections, we introduced two encoder structures that encode global and local information, respectively. How to effectively use the feature information extracted by the encoder and decode it accurately is the main goal of the decoder network introduced in this section. In the process of continuous feature extraction layer by layer in the coded network, the low-level information of the feature map is continuously filtered and the high-level information is extracted. If the segmentation results are reconstructed directly based on the sampling of coded features, the network cannot learn the detailed feature information effectively. UNet uses skip connections to conduct the feature maps of the encoding module of each stage to the decoding module of the corresponding stage, and the network can fully learn the feature maps of different levels of the image. We adopted the skip connection operation from UNet and introduced skip connections to different feature encoders to allow the whole network to better learn the feature information of different encoders at different levels. The skip connection introduced in the local feature encoder is similar to the traditional UNet module, which combines the short-range skip connection (residual connection) and the long-range skip connection of SEBottleNet. The high-level features continue to enrich the network's perception of low-level in the extraction process, and finally the output feature map has a more refined feature representation. In the decoding process of the global feature encoder, we first introduce skip connections in the encoding process of the backbone network to connect the intermediate feature maps in the forward propagation process of the backbone embedding network to the corresponding stage of the decoder, which improves the low-level feature loss in the encoding embedding process of the backbone network. Next, we add skip connections to the feature maps with global feature representations after Transformer feature encoding fusion to fuse the global low-level features. Eventually, after continuously fusing low-level feature maps of different scales, the decoder can learn the semantic information of images from coarse to fine.

### 2.4 Applying transfer learning to TransFusionNet

The TransFusionNet can significantly learn full-resolution context feature information, and its segmentation effect in the public dataset of blood vessels and liver tumors is significant. However, due to the scarcity of the enhanced CT images of liver cancer after the screening, we only obtained CT images of 18 patients. Too little data will inevitably affect the performance of the model and deepen the over-fitting problem. For this purpose we introduce a transfer learning strategy, which does not require exactly representative training data and is able to take advantage of the similarity between datasets to capture specific prior knowledge during the training phase of the model in order to construct new segmentation models.

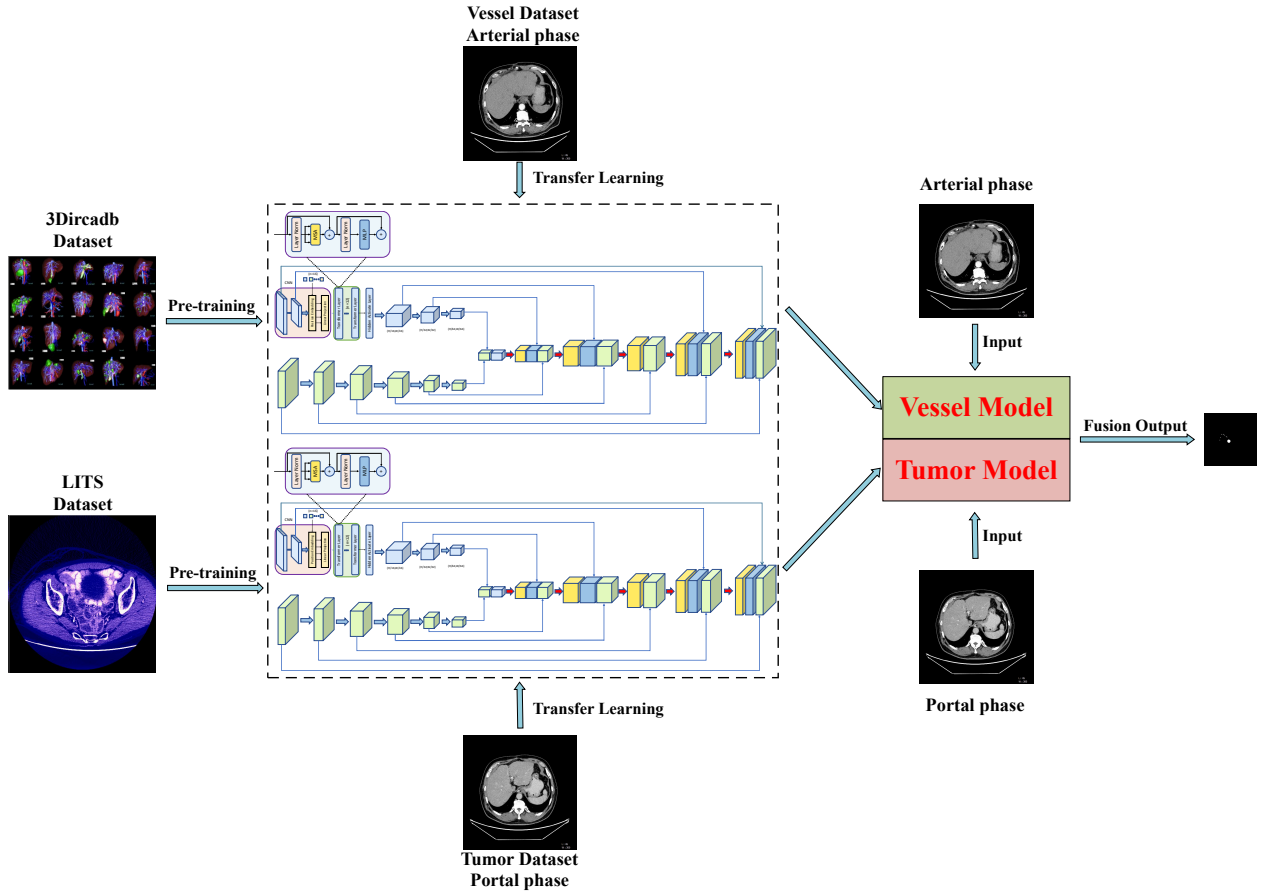


Figure 3: Transfer learning strategy using TransFusionNet

Our schematic diagram of transfer learning for TransFusionNet is shown in Figure 3. We first pre-trained the models using the publicly available datasets LITS and 3Dircadb to obtain a liver tumor segmentation model and a liver vascular segmentation model, respectively. Then, we use our liver tumor data and liver vascular data to retrain the two models obtained by pre-training, and obtain two liver tumor segmentation models and liver vascular segmentation models based on the training sample distribution of our dataset. When we need to perform segmentation of liver tumor and blood vessels of CT images, we only need to input one CT image, and the two models will segment the tumor and blood vessel parts of CT images respectively. The mask output from the two model segments is automatically fused into a single mask that contains the tumor and blood vessels with relative positions as the final output.

### 3 Experiment and discussion

We use PyTorch to implement our proposed model and integrate all the comparison experiments in the same code to complete it. We set the epoch to 150, the initial learning rate to 0.001 (using the cosine annealing learning rate decay method), and the batch size to 4. The model is trained using an SGD optimizer with a momentum of 0.9 and a weight decay of 1e-4. For the parameters of the Transformer global encoder, we use 12 ViT-based[32] Transformer layers; for the parameters of the SEBottleNet local feature encoder, we use 3 convolutional layers and one SE layer. For equipment, we use 1 Intel(R) Xeon(R) Gold 6226R 2.90GHz CPU and 1 NVIDIA Tesla V100 gpu server for our experiments.

### 3.1 Experimental setup

#### 3.1.1 Dataset

The LITS (Liver and Liver Tumor Segmentation) dataset contains 130 cases of tumors, metastases, and cysts, and these CT scans have large spatial resolution and field of view (FOV) differences[6]. 3Dircadb (3D Image Reconstruction for Comparison of Algorithm Database) is a public dataset that can be used to train and test liver vessel segmentation methods, including 20 patients in different image resolutions, vessel structure, intensity distribution and liver vessel comparison CT enhancement[23]. At the same time, we collected 18 typical patients' portal and arterial phase CT enhanced images of the liver for manual annotation, and finally constructed a liver tumor blood vessel(LTBV) dataset. We annotated the hepatic arterial vessels in the arterial phase images of the same patient and annotated the liver tumors in the portal phase images. Due to the different characteristics of CT images in the two phases, we need to train two models for automatic segmentation of arterial vessels and tumors.

The LITS and 3Dircadb datasets cover a wide range of CT images with different resolution differences and field of view (FOV) differences. We use these two datasets for model pre-training. We use our private dataset for the fine-tuning training of the model for hepatic artery and tumor segmentation tasks. The above three datasets are divided into training set and test set according to the ratio of 8:2.

#### 3.1.2 Evaluation Metrics

In order to better evaluate our model from multiple perspectives, we have selected 5 evaluation indicators including: iou, DSC coefficient, voe, recall, precision.

IoU(Intersection over Union) is the calculation of the intersection of the real annotation and the segmentation result. The calculation method was

$$IoU = \frac{R_{pre} \cap R_{real}}{R_{pre} \cup R_{real}}, \quad (6)$$

where  $R_{pre}$  represents the segmentation result predicted by the model, and  $R_{real}$  represents the actual segmentation result. The DSC(Dice Similariy Coefficient) represents the ratio of the area where the segmented image and the real image intersect to the total area. The calculation method was

$$DSC = \frac{2 \times (R_{pre} \cap R_{real})}{R_{pre} + R_{real}}, \quad (7)$$

where  $R_{pre}$  represents the segmentation result predicted by the model, and  $R_{real}$  represents the actual segmentation result. VOE(Volumetric Overlap Error) represents the difference between the area of the segmented image and the real image, and usually represents the error rate of segmentation. The specific calculation method was

$$VOE = \frac{2 \times (R_{pre} - R_{real})}{R_{pre} + R_{real}}. \quad (8)$$

Precision is the proportion of pixels that are actually not in the region of interest correctly judged as not in the region of interest. It measures the ability to correctly judge the pixels that are not in the region of interest in the segmentation experiment. Its calculation method was

$$Precision = \frac{I - R_{pre} \cup R_{real}}{I - R_{real}}. \quad (9)$$

Where I is the original input image. Recall is the proportion of pixels that are correctly judged as pixels in the region of interest. It measures the ability to correctly segment the region of interest. Its calculation method was

$$Recall = \frac{R_{pre} \cap R_{real}}{R_{real}}. \quad (10)$$

### 3.2 Performance comparison with state-of-the-art methods

We choose 4 advanced segmentation models to compare with our method, the 4 models are SegNet[18], UNet[22], UNet++[24], TransUNet[33]. We first compare the segmentation effects of five models on blood vessels and tumors based on two public datasets:LITS(Tumor)and 3Dircadb(Vessel). Next, we use the LTBV dataset to fine-tune the five models and compare the segmentation effects of the five models.

### 3.2.1 Comparison experiment of liver tumor and blood vessel segmentation effects based on public datasets:LITS and 3Dircadb

The performance of TransFusionNet and the other four methods on two public datasets is shown in Table 1. The experimental results show that the IoU of TransFusionNet on the 3Dircadb dataset can reach 0.854, and the DSC can reach 0.918, which is 0.8% and 1.1% higher than the IoU and DSC of the baseline method UNet. The IoU is 2.3% and 0.7% higher than UNet++ and TransUNet, respectively. On the LITS dataset, that is, when performing liver tumor segmentation, the IoU and DSC of TransFusionNet can reach 0.840 and 0.910. As can be seen from Table 1, the VOE of TransFusionNet on the two datasets, that is, the error rate is also far lower For other models. In summary, our model performs best in the segmentation of liver blood vessels and liver tumors.

Table 1: Performance comparison of TransFusionNet and other methods on LITS and 3Dircadb datasets

| Dataset  | Methods     | IoU          | DSC          | VOE           | Precision    | Recall       |
|----------|-------------|--------------|--------------|---------------|--------------|--------------|
| 3Dircadb | SegNet      | 0.839        | 0.907        | -0.067        | 0.938        | 0.879        |
|          | UNet        | 0.846        | 0.913        | -0.079        | <b>0.951</b> | 0.880        |
|          | UNet++      | 0.831        | 0.904        | -0.062        | 0.934        | 0.879        |
|          | TransUNet   | 0.847        | 0.913        | -0.066        | 0.944        | 0.885        |
|          | <b>Ours</b> | <b>0.854</b> | <b>0.918</b> | <b>-0.041</b> | 0.938        | <b>0.901</b> |
| LITS     | SegNet      | 0.805        | 0.887        | -0.035        | 0.904        | 0.875        |
|          | UNet        | 0.832        | 0.905        | -0.024        | 0.917        | 0.897        |
|          | UNet++      | 0.828        | 0.902        | -0.020        | 0.912        | 0.896        |
|          | TransUNet   | 0.834        | 0.905        | -0.040        | 0.923        | 0.889        |
|          | <b>Ours</b> | <b>0.840</b> | <b>0.910</b> | <b>-0.018</b> | <b>0.919</b> | <b>0.904</b> |

### 3.2.2 Comparison experiment of liver tumor and blood vessel segmentation effects based on private dataset:LTBV

As the experiments described in section 3.2.1, we used LITS and 3Dircadb public datasets to train to obtain segmentation models of liver tumors and blood vessels. Compared with the other four state-of-the-art methods, our method has the best automatic segmentation effect. We use five methods trained on two datasets to perform transfer learning fine-tuning training on the LTBV dataset. The performance of each model in the LTBV dataset as shown in Table 2. From Table 2, we can see that the IoU of TransFusionNet on the blood vessel dataset can reach 0.822, and the DSC can reach 0.899. This is 1.9% and 1.8% higher than the IoU and DSC of the baseline method SegNet, and is higher than the IoU and Voe of TransUNet. They are 0.4% and 0.5% higher respectively. On the tumor dataset, the IoU and DSC of TransFusionNet are as high as 0.927 and 0.961, which shows our method can still achieve the best results after LTBV transfer learning.

Table 2: Performance comparison of TransFusionNet and other methods on LTBV datasets

| Dataset | Methods     | IoU          | DSC          | VOE           | Precision    | Recall       |
|---------|-------------|--------------|--------------|---------------|--------------|--------------|
| Vessel  | SegNet      | 0.803        | 0.881        | -0.056        | 0.907        | 0.858        |
|         | UNet        | 0.812        | 0.893        | <b>-0.013</b> | 0.902        | 0.890        |
|         | UNet++      | 0.809        | 0.892        | -0.058        | 0.919        | 0.868        |
|         | TransUNet   | 0.818        | 0.897        | -0.049        | 0.920        | 0.876        |
|         | <b>Ours</b> | <b>0.822</b> | <b>0.899</b> | -0.054        | <b>0.925</b> | <b>0.877</b> |
| Tumor   | SegNet      | 0.905        | 0.948        | 0.002         | 0.922        | 0.931        |
|         | UNet        | 0.915        | 0.954        | -0.018        | 0.963        | 0.946        |
|         | UNet++      | 0.912        | 0.952        | 0.003         | 0.952        | 0.954        |
|         | TransUNet   | 0.920        | 0.955        | -0.023        | <b>0.967</b> | 0.945        |
|         | <b>Ours</b> | <b>0.927</b> | <b>0.961</b> | <b>-0.011</b> | 0.966        | <b>0.955</b> |

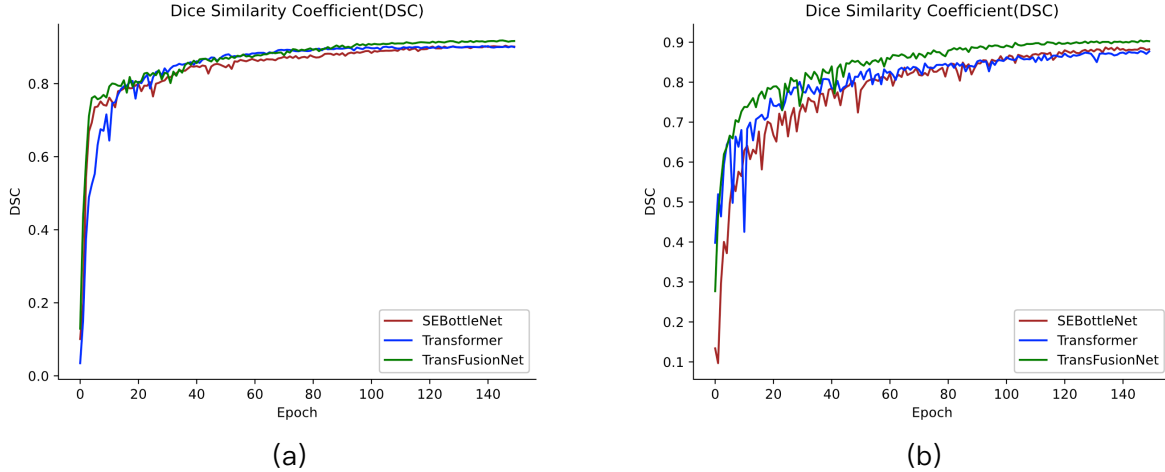


Figure 4: Performance of Transformer global encoder, SEBottleNet local encoder and TransFusionNet on (a) 3Dircadb dataset and (b) LITS dataset.

### 3.3 Ablation Study for TransFusionNet model

#### 3.3.1 Ablation study of Transformer-based global encoder and SEBottleNet local encoder

In this section, we use the Transformer module, the SEBottleNet module, and TransFusionNet for our experiments, with the aim of testing the effect of the above two modules on the segmentation accuracy of TransFusionNet. From Figure 4(a) we can see that the Transformer module performs better than the SEBottleNet module in general on the vascular dataset of 3Dircadb. We believe that the Transformer encoder can learn the CT image global contextual feature representation, especially it encodes the image location information, which certainly helps to enhance the segmentation of the image as a whole. On the LITS tumor dataset, as shown in Figure 4(b), the segmentation accuracy of the SEBottleNet module is higher, which is attributed to the fact that its internal CNN and local residuals are more interested in some finer features in the image, such as tumor edge features. From Figure 4, we can see that this paper achieves an effective improvement in the segmentation accuracy of liver vessels and tumors by combining the Transformer module and SEBottleNet module.

#### 3.3.2 Function of skip connection used in Decooder

In the Encoder-Decoder structure, the encoder learns to extract the high-frequency image representation of the feature map, and the decoder continuously learns feature recovery based only on the high-frequency feature coding output from the encoder. The role of low-frequency feature information is ignored in the process of encoding and decoding, yet low-frequency features often have their non-negligible role. The role of skip connection is to allow the network to better learn low-frequency features during the encoding and decoding process. In this experiment, to demonstrate the importance of different modular jump links of our designed network on the segmentation effect, we remove the skip connections of the global encoder network, the skip connections of the local encoder network and all skip connections, and train these three models using the same parameter settings. The performance gap with the original network is compared. The experimental results are shown in Table 3. According to the results in the Table 3, we can find that the model retaining the global local skip connections has a significant improvement compared to the model with the jump links removed. This result proves the importance of skip connections for TransFusionNet and also shows that the low frequency features of the image have a significant impact on the segmentation results.

### 3.4 Visualizations

From the above quantitative experimental methods, our model has the best performance in the segmentation of liver blood vessels and liver tumors. Next, we use TransFusionNet and other comparable models on a test case on the LTBV dataset to segment liver tumors and blood vessels and then visualize them. The first row of Figure 4 is the model's

Table 3: Performance comparison of TransFusionNet and other methods on LITS and 3Dircadb datasets

| Dataset  | Modules without skip connections | IoU          | DSC          | VOE           | Precision    | Recall       |
|----------|----------------------------------|--------------|--------------|---------------|--------------|--------------|
| 3Dircadb | all encoders                     | 0.654        | 0.780        | -0.163        | 0.862        | 0.732        |
|          | Transformer-based encoder        | 0.767        | 0.858        | 0.059         | 1.066        | 0.886        |
|          | CNN-based encoder                | 0.785        | 0.870        | 0.019         | 0.880        | 0.868        |
|          | <b>Ours</b>                      | <b>0.854</b> | <b>0.918</b> | <b>-0.041</b> | <b>0.938</b> | <b>0.901</b> |
| LITS     | all encoders                     | 0.805        | 0.887        | -0.035        | 0.904        | 0.875        |
|          | Transformer-based encoder        | 0.832        | 0.905        | -0.024        | 0.917        | 0.897        |
|          | CNN-based encoder                | 0.828        | 0.902        | -0.020        | 0.912        | 0.896        |
|          | <b>Ours</b>                      | <b>0.840</b> | <b>0.910</b> | <b>-0.018</b> | <b>0.919</b> | <b>0.904</b> |

segmentation of Vessel, the second row is the model’s segmentation of Tumor, and the third row is the result of fusing the first two rows of segmentation results in the same coordinate system.

From the perspective of visual analysis, SegNet and UNet are not accurate in segmenting the details of blood vessels. Although UNet++ can identify some details of blood vessels, the error rate is too high. TransFusionNet almost perfectly segmented the details of blood vessels, which is more accurate than TransUNet. This is attributed to SEBottleNet’s extraction of local receptive field information and the importance of different channels. In tumor segmentation, UNet++ has a great segmentation result for the edge of the tumor, while SegNet and UNet perform poorly in this respect. All comparison models have some wrong tumor segmentation, and TransFusionNet not only avoids these wrong segmentation but also can segment the edge and contour of the tumor accurately. We believe that after TransFusionNet extracts global and local information, the multi-scale feature fusion decoder almost perfectly restores the feature of the image, so that the segmentation accuracy is significantly improved, and the error rate is low.

In summary, the above comparison models are not accurate in segmenting tumors and blood vessels. They are easy to misclassify some areas that are not tumors, and they are not sensitive to the recognition of some fine blood vessels areas, resulting in incomplete blood vessel segmentation results. TransFusionNet can accurately segment the liver tumor regardless of its integrity or vascular continuity.

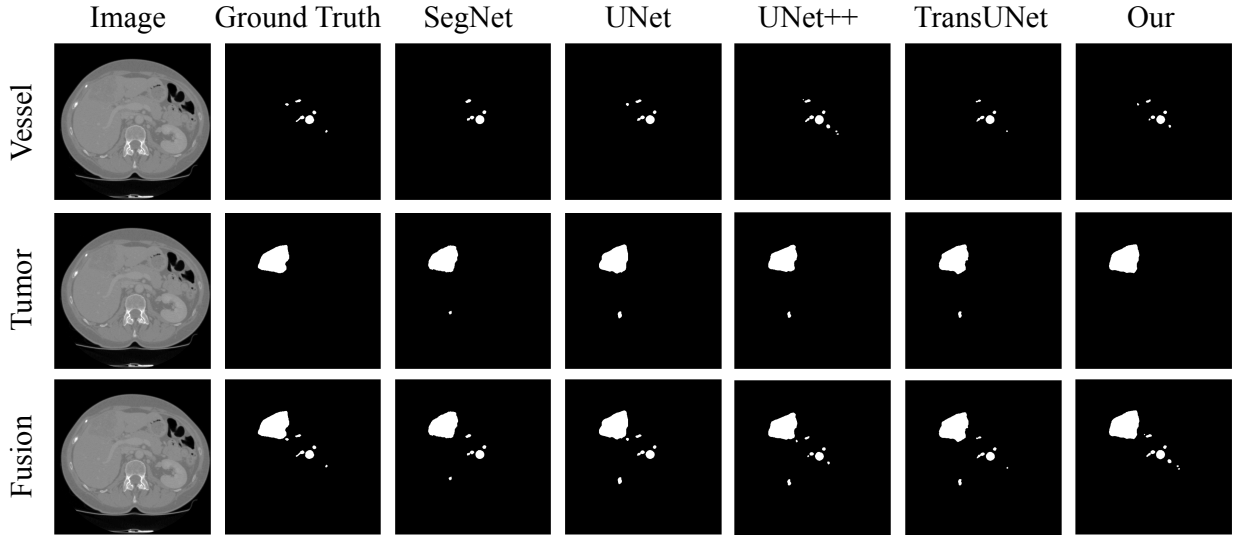


Figure 5: Qualitative analysis of the 2D segmentation results of blood vessels, tumors and fusions of TransFusionNet and other comparison models from visual perspective

### 3.5 Case Study: Automated 3D Reconstruction of Liver Tumor Vessels Using TransfusionNet

#### 3.5.1 Detail of the reconstruction algorithm

Medical image segmentation has a wide range of applications and research values in medical research and practice fields such as medical research, clinical diagnosis, pathological analysis, computer-assisted surgery, and three-dimensional simulations. In this section, we implement automatic segmentation of tumors and arteries for some typical liver cancer patients and use 3DSlicer to perform a 3D reconstruction task on the segmentation results. An integrated reconstruction algorithm is constructed by combining model prediction with result reconstruction. The detailed algorithm implementation is shown in algorithm 1.

The algorithm input is the arterial phase CT-enhanced image  $a \in \mathbb{R}^{N \times C \times H \times W}$ , the portal venous phase CT-enhanced image  $p \in \mathbb{R}^{N \times C \times H \times W}$ , the segmentation model  $\mathcal{F} : \mathbb{R}^{N \times C \times H \times W} \rightarrow \mathbb{R}^{N \times H \times W}$  for predicting liver tumors, and the segmentation model  $\mathcal{G} : \mathbb{R}^{N \times C \times H \times W} \rightarrow \mathbb{R}^{N \times H \times W}$  for predicting arterial blood vessels. The algorithm first feeds  $a$  into  $\mathcal{G}$  to predict the blood vessel segmentation  $\mathcal{O}_v$ . Next, the  $p$  feed into  $\mathcal{F}$  to predict  $\mathcal{O}_t$ . Finally, an integration algorithm was implemented to integrate  $\mathcal{O}_t$  and  $\mathcal{O}_v$  and obtain the 3D reconstruction result  $\mathcal{O}'_i$ . The details of the Integration algorithm are shown in Algorithm 2. To support the 3DSlicer reconstruction interface,  $\mathcal{O}'_i$  was saved as `.nrrd` format, which consists of a data header and stored data in a three-dimensional array format. The data header is a python dictionary format that contains information such as the dimension of the data, CT image spacing, segment label value, segment color, and the encoding method. Some important settings in the data header are

```
{
  "dimension" : 3,
  "sizes" : [512,512,374],
  "space directions" : array([[0.816406, 0., 0.],[0., 0.816406, 0.],[0., 0., 1.25]]),
  "encoding": "gzip",
  "Segment0_Color" : "0.501961 0.682353 0.501961",
  "Segment0_ColorAutoGenerated" : "1",
  "Segment0_ID" : "Segment_1",
  "Segment0_LabelValue" : "1",
  "Segment0_Layer" : "0",
  "Segment0_Name" : "tumor",
  "Segment0_NameAutoGenerated" : "1",
}.
```

In this example, the reconstruction result satisfies  $\mathcal{O}'_i \in \mathbb{R}^{512 \times 512 \times 314}$ , and its spacing in each direction is 0.816, 0.816, and 1.25, respectively. In  $\mathcal{O}'_i$ , there is a segmented area named "tumor" with a value of 1, and the rendering color in 3DSlicer is a [0.501961, 0.682353, 0.501961] RGB color.

In algorithm 2, the input is the prediction results  $\mathcal{O}_t$ ,  $\mathcal{O}_v$  and filter thresholds  $\xi$ , the output is the reconstruction result  $\mathcal{O}_i$ . The algorithm first filters the each layers of prediction results in  $\mathcal{O}_t$  and  $\mathcal{O}_v$  respectively according to  $\xi$ . In this process, firstly, the pixels greater than  $\xi$  in each layer of  $\mathcal{O}_t$  are set to 1, otherwise set to 0; Next, set the pixels greater than  $\xi$  in each layer of  $\mathcal{O}_v$  to 2, otherwise set to 0. The implementation is mainly in the description of step 3-17 in algorithm, in which the `numpy.where` function of array operation can be used instead of for loop to improve the efficiency of filtering. After filtering, the region of interest of the two results is combined using a merge operation. The specific implementation is shown in Step 20 of Algorithm 2. In short, this step is a pixel-wise add operation for  $\mathcal{O}_v$  and  $\mathcal{O}_t$ , where  $\mathcal{O}_v$  represent a layer of  $\mathcal{O}_v$  and  $\mathcal{O}_t$  represent a layer of  $\mathcal{O}_t$ . Since the two stages of CT data came from the same patient, the positional relationship between the tumor and the blood vessel can be guaranteed by combining the two results. The modification can effectively fuse the predict label of tumors and blood vessels, and its implementation is shown in Algorithm 3. When a region of interest of tumor and blood vessel coincides, the summed result becomes 3 at the pixel value of the corresponding location, which actually belongs to the blood vessel in the tumor. We therefore define a modification algorithm that sets the region of the resulting pixel value of 3 to 2 and returns the modified result. By doing the above steps for each layer of segment results and stacking the results of each step, the output of the integrated algorithm can be obtained.

**Algorithm 1** Reconstruction( $a, p, \mathcal{F}, \mathcal{G}, \xi$ )**Input:**

arterial phase CT image sequences,  $a \in \mathbb{R}^{N \times C \times H \times W}$ ;  
 portal venous phase CT image sequences,  $p \in \mathbb{R}^{N \times C \times H \times W}$ ;  
 $\mathcal{F}$ :  $\mathbb{R}^{N \times C \times H \times W} \rightarrow \mathbb{R}^{N \times H \times W}$ ;  
 $\mathcal{G}$ :  $\mathbb{R}^{N \times C \times H \times W} \rightarrow \mathbb{R}^{N \times H \times W}$ ;  
 Threshold for filter the mask,  $\xi$ ;

**Output:**

3D reconstruction results of liver tumors and blood vessels,  $\mathcal{O}'_i$ ;  
 1: // Apply liver tumor segmentation model to predict the mask of portal venous phase image  
 2:  $\mathcal{O}_t = \mathcal{G}(p)$   
 3: // Apply liver vessel segmentation model to predict the mask of liver arterial phase image  
 4:  $\mathcal{O}_v = \mathcal{F}(a)$   
 5:  $\mathcal{O}_i = \text{Integration}(\mathcal{O}_t, \mathcal{O}_v)$   
 6: Reformat  $\mathcal{O}_i$  to a reconstruction format supported by the 3DSlicer. This step finally outputs the reconstruction result  $\mathcal{O}'_i$

**Algorithm 2** Integration( $\mathcal{O}_t, \mathcal{O}_v, \xi$ )**Input:**

Segmentation prediction results for liver tumors by TransfusionNet,  $\mathcal{O}_t \in \mathbb{R}^{N \times H \times W}$ ;  
 Segmentation prediction results for liver arterial vessel by TransfusionNet,  $\mathcal{O}_v \in \mathbb{R}^{N \times H \times W}$ ;  
 Threshold for filter the mask,  $\xi$ ;

**Output:**

3D reconstruction results of liver tumors and blood vessels,  $\mathcal{O}_i$ ;  
 1: Initialize empty vector  $\mathcal{O}_i = \{\}$   
 2: **for** each masks( $o_t, o_v \in \mathbb{R}^{H \times W}$ ) in the prediction result( $\mathcal{O}_t, \mathcal{O}_v$ ) in a batch **do**  
 3: // Filter the pixels of the mask  $o_t$  according to the threshold  $\xi$   
 4: **for** each pixels  $i$  in mask  $o_t$  **do**  
 5:   **if**  $i \geq \xi$  **then**  
 6:     set  $i = 1$   
 7:   **else**  
 8:     set  $i = 0$   
 9:   **end if**  
 10: **end for**  
 11: // Filter the pixels of the mask  $o_v$  according to the threshold  $\xi$   
 12: **for** each pixels  $j$  in mask  $o_v$  **do**  
 13:   **if**  $i \geq \xi$  **then**  
 14:     set  $j = 2$   
 15:   **else**  
 16:     set  $j = 0$   
 17:   **end if**  
 18: **end for**  
 19: // pixel-wise add for masks  $o_v$  and  $o_t$   
 20:  $\mathcal{O}_i = o_t + o_v$   
 21:  $\mathcal{O}'_i = \text{modification}(\mathcal{O}_i)$   
 22:  $\mathcal{O}_i = \mathcal{O}_i \cup \{\mathcal{O}'_i\}$   
 23: **end for**

**3.5.2 Reconstruction Result**

Through performance analysis, our automatic reconstruction algorithm can be completed within 1s on a workstation equipped with NVIDIA RTX3090 computing unit. At the same time, we compared the results of the automatic reconstruction with the results of manual annotation. The Figure 6 shows a comparison between the reconstruction results and manual annotations of a typical patient. Except for some noise and loss of vessel details, the reconstruction results were very close to the actual annotation results. However, a detailed manual annotation requires a lot of time and effort, which significantly reflect the efficiency and accuracy of our proposed algorithm.

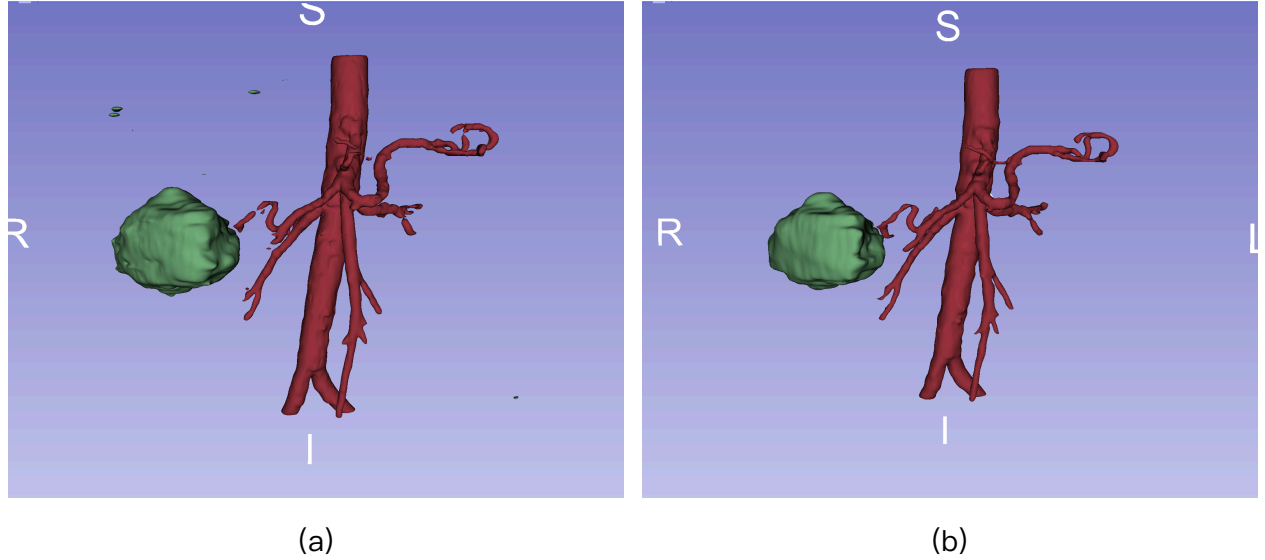
**Algorithm 3** modification( $o_i$ )**Input:**The result of pixel-wise add for masks,  $o_i$ ;**Output:**The final modified result,  $o_i$ ;1: Traverse each pixel in the mask  $o_i$ , and modify the pixel to 2 with the value of 3 in the mask  $o_i$ .2: Return the modified mask result  $o'_i$ .

Figure 6: Visual comparison of reconstruction results. (a) Reconstruction result using automatic reconstruction algorithm. (b) Reconstruction results using manual annotations

## 4 conclusion

In this work, we propose a segmentation model which can effectively extract the full-scale feature information of CT images. The IOU reached the peak performance of 0.854 in the vessel segmentation of the public dataset 3dircadb and 0.840 in the liver tumor segmentation of the public dataset LITS. At the same time, we transferred the trained model to our annotated dataset, and the IOU in tumor and vascular segmentation reached 0.927 and 0.822 respectively. Compared with the state-of-the-art segmentation methods, TransFusionNet has an accuracy improvement of 1% - 2%. Although this experiment is only for the segmentation of liver tumors and blood vessels, our model can also be applied to the segmentation of other tissues.

To further illustrate the segmentation capability of our segmentation algorithm for liver tumors and blood vessels, we propose an automatic reconstruction algorithm, which makes further 3D reconstruction based on the segmentation results of TransFusionNet. By comparing the reconstruction results with the real annotated reconstruction results, TransFusionNet can accurately grasp the morphology of blood vessels and tumors and complete specific reconstruction. This further proves the segmentation accuracy of TransFusionNet for liver tumors and blood vessels. At the same time, the reconstruction of liver tumors and blood vessels can be completed in a short time by using our proposed reconstruction algorithm. Contrasted with the traditional reconstruction algorithm, it greatly reduces the operation time and facilitates the follow-up surgical treatment and pathological analysis of doctors.

Although we have completed the reconstruction of liver tumors and blood vessels, the segmentation and reconstruction of intrahepatic blood vessels using our method still needs to be further improved. Due to the numerous and small branches of intrahepatic vessels, it is difficult for deep learning algorithm to perceive the characteristics of intrahepatic vessels. At the same time, the clarity of CT image will also hinder the fine reconstruction of internal hepatic artery. Facing so many challenges, in the next work, we will try to use hydrodynamic calculation method to further restore and repair the reconstruction results.

## References

- [1] Xin Li, Pierluigi Ramadori, Dominik Pfister, Marco Seehawer, Lars Zender, and Mathias Heikenwalder. The immunological and metabolic landscape in primary and metastatic liver cancer. *Nature Reviews Cancer*, pages 1–17, 2021.
- [2] Debra A Gervais, S Nahum Goldberg, Daniel B Brown, Michael C Soulen, Steven F Millward, and Dheeraj K Rajan. Society of interventional radiology position statement on percutaneous radiofrequency ablation for the treatment of liver tumors. *Journal of Vascular and Interventional Radiology*, 20(7):S342–S347, 2009.
- [3] Marcin Ciechlewski and Michał Kassjański. Computational methods for liver vessel segmentation in medical imaging: A review. *Sensors*, 21(6):2027, 2021.
- [4] Qingsen Yan, Bo Wang, Wei Zhang, Chuan Luo, Wei Xu, Zhengqing Xu, Yanning Zhang, Qinfeng Shi, Liang Zhang, and Zheng You. An attention-guided deep neural network with multi-scale feature fusion for liver vessel segmentation. *IEEE Journal of Biomedical and Health Informatics*, 2020.
- [5] Huang-Wen Huang. Influence of blood vessel on the thermal lesion formation during radiofrequency ablation for liver tumors. *Medical physics*, 40(7):073303, 2013.
- [6] Huiyan Jiang, Tianyu Shi, Zhiqi Bai, and Liangliang Huang. Ahcnet: An application of attention mechanism and hybrid connection for liver tumor segmentation in ct volumes. *IEEE Access*, 7:24898–24909, 2019.
- [7] Yuanzhi Cheng, Xin Hu, Ji Wang, Yadong Wang, and Shinichi Tamura. Accurate vessel segmentation with constrained b-snake. *IEEE Transactions on Image Processing*, 24(8):2440–2455, 2015.
- [8] Minyoung Chung, Jeongjin Lee, Jin Wook Chung, and Yeong-Gil Shin. Accurate liver vessel segmentation via active contour model with dense vessel candidates. *Computer methods and programs in biomedicine*, 166:61–75, 2018.
- [9] Christian Bauer, Thomas Pock, Erich Sorantin, Horst Bischof, and Reinhard Beichel. Segmentation of interwoven 3d tubular tree structures utilizing shape priors and graph cuts. *Medical image analysis*, 14(2):172–184, 2010.
- [10] Simon Esneault, Cyril Lafon, and Jean-Louis Dillenseger. Liver vessels segmentation using a hybrid geometrical moments/graph cuts method. *IEEE Transactions on Biomedical Engineering*, 57(2):276–283, 2009.
- [11] Marie-Ange Lebre, Antoine Vacant, Manuel Grand-Brochier, Hugo Rositi, Armand Abergel, Pascal Chabrot, and Benoit Magnin. Automatic segmentation methods for liver and hepatic vessels from ct and mri volumes, applied to the couinaud scheme. *Computers in biology and medicine*, 110:42–51, 2019.
- [12] Jens N Kaftan, Hüseyin Tek, and Til Aach. A two-stage approach for fully automatic segmentation of venous vascular structures in liver ct images. In *Medical imaging 2009: image processing*, volume 7259, page 725911. International Society for Optics and Photonics, 2009.
- [13] Ye-zhan Zeng, Yu-qian Zhao, Ping Tang, Miao Liao, Yi-xiong Liang, Sheng-hui Liao, and Bei-ji Zou. Liver vessel segmentation and identification based on oriented flux symmetry and graph cuts. *Computer methods and programs in biomedicine*, 150:31–39, 2017.
- [14] Dwarikanath Mahapatra. Analyzing training information from random forests for improved image segmentation. *IEEE Transactions on Image Processing*, 23(4):1504–1512, 2014.
- [15] A Smith. Image segmentation scale parameter optimization and land cover classification using the random forest algorithm. *Journal of Spatial Science*, 55(1):69–79, 2010.
- [16] XY Wanga, T Wang, and J Bua. Color image segmentation using pixel wise structural-support-vector-machine (s-svm) classification. *Pattern Recognit*, 44(4):777–787, 2011.
- [17] Yu Zhiwen, HS Wong, and Wen Guihua. A modified support vector machine and its application to image segmentation [j]. *Image and Vision Computing*, 29(1):29–40, 2011.
- [18] Vijay Badrinarayanan, Alex Kendall, and Roberto Cipolla. Segnet: A deep convolutional encoder-decoder architecture for image segmentation. *IEEE transactions on pattern analysis and machine intelligence*, 39(12):2481–2495, 2017.
- [19] Sibo Qiao, Shanchen Pang, Min Wang, Xue Zhai, Shihang Yu, and Tong Ding. A convolutional neural network for brain ct image classification based on residual hybrid attention mechanism. *ACTA ELECTRONICA SINICA*, 49(5):984, 2021.
- [20] Xiangyu Meng, Xin Li, and Xun Wang. A computationally virtual histological staining method to ovarian cancer tissue by deep generative adversarial networks. *Computational and Mathematical Methods in Medicine*, 2021, 2021.

- [21] Jonathan Long, Evan Shelhamer, and Trevor Darrell. Fully convolutional networks for semantic segmentation. In *Proceedings of the IEEE conference on computer vision and pattern recognition*, pages 3431–3440, 2015.
- [22] Olaf Ronneberger, Philipp Fischer, and Thomas Brox. U-net: Convolutional networks for biomedical image segmentation. In *International Conference on Medical image computing and computer-assisted intervention*, pages 234–241. Springer, 2015.
- [23] Qing Huang, Jinfeng Sun, Hui Ding, Xiaodong Wang, and Guangzhi Wang. Robust liver vessel extraction using 3d u-net with variant dice loss function. *Computers in biology and medicine*, 101:153–162, 2018.
- [24] Zongwei Zhou, Md Mahfuzur Rahman Siddiquee, Nima Tajbakhsh, and Jianming Liang. Unet++: A nested u-net architecture for medical image segmentation. In *Deep learning in medical image analysis and multimodal learning for clinical decision support*, pages 3–11. Springer, 2018.
- [25] Ashish Vaswani, Noam Shazeer, Niki Parmar, Jakob Uszkoreit, Llion Jones, Aidan N Gomez, Łukasz Kaiser, and Illia Polosukhin. Attention is all you need. In *Advances in neural information processing systems*, pages 5998–6008, 2017.
- [26] Chen Li, Yusong Tan, Wei Chen, Xin Luo, Yulin He, Yuanming Gao, and Fei Li. Anu-net: Attention-based nested u-net to exploit full resolution features for medical image segmentation. *Computers & Graphics*, 90:11–20, 2020.
- [27] Debesh Jha, Michael A Riegler, Dag Johansen, Pål Halvorsen, and Håvard D Johansen. Doubleu-net: A deep convolutional neural network for medical image segmentation. In *2020 IEEE 33rd International symposium on computer-based medical systems (CBMS)*, pages 558–564. IEEE, 2020.
- [28] Tao Song, Fan Meng, Alfonso Rodriguez-Paton, Pibao Li, Pan Zheng, and Xun Wang. U-next: a novel convolution neural network with an aggregation u-net architecture for gallstone segmentation in ct images. *IEEE Access*, 7:166823–166832, 2019.
- [29] Annegreet Van Opbroek, M Arfan Ikram, Meike W Vernooij, and Marleen De Bruijne. Transfer learning improves supervised image segmentation across imaging protocols. *IEEE transactions on medical imaging*, 34(5):1018–1030, 2014.
- [30] Kaiming He, Xiangyu Zhang, Shaoqing Ren, and Jian Sun. Identity mappings in deep residual networks. In *European conference on computer vision*, pages 630–645. Springer, 2016.
- [31] Jie Hu, Li Shen, and Gang Sun. Squeeze-and-excitation networks. In *Proceedings of the IEEE conference on computer vision and pattern recognition*, pages 7132–7141, 2018.
- [32] Alexey Dosovitskiy, Lucas Beyer, Alexander Kolesnikov, Dirk Weissenborn, Xiaohua Zhai, Thomas Unterthiner, Mostafa Dehghani, Matthias Minderer, Georg Heigold, Sylvain Gelly, et al. An image is worth 16x16 words: Transformers for image recognition at scale. *arXiv preprint arXiv:2010.11929*, 2020.
- [33] Jieneng Chen, Yongyi Lu, Qihang Yu, Xiangde Luo, Ehsan Adeli, Yan Wang, Le Lu, Alan L Yuille, and Yuyin Zhou. Transunet: Transformers make strong encoders for medical image segmentation. *arXiv preprint arXiv:2102.04306*, 2021.